



Simultaneous In Situ Measurement of Temperature and Relative Humidity in a PEMFC Using Optical Fiber Sensors

N. A. David,^{a,z} P. M. Wild,^{a,*} J. Jensen,^a T. Navessin,^b and N. Djilali^{a,*}

^aDepartment of Mechanical Engineering and Institute for Integrated Energy Systems, University of Victoria, British Columbia, Canada V8W 3P6

^bNational Research Council Institute for Fuel Cell Innovation, Vancouver, British Columbia, Canada V6T 1W5

The development, implementation, and demonstration of in-fiber Bragg grating (FBG) sensors for a simultaneous measurement of temperature and relative humidity (RH) in an operating polymer electrolyte membrane fuel cell (PEMFC) are presented. Etched fiber, polymer-coated FBG sensors with fast response and high sensitivity are installed in situ in a minimally invasive manner in the cathode unipolar plate of a single PEMFC with serpentine flow fields. The performance of the fuel cell under transient operating conditions is monitored. Step increases in current induce significantly larger increases in RH near the outlet than near the inlet of the cell, and associated transients within the fuel cell are found on a time scale approaching the sensor response time (~ 1 Hz). The improved response of the technique, together with the significantly improved temperature and RH resolution, provides useful information on the dynamics of heat and water management. The technique is well suited for distributed measurements, and its relatively low cost and nonintrusive character make it a good candidate for practical multipoint monitoring of complete stacks.

© 2010 The Electrochemical Society. [DOI: 10.1149/1.3436652] All rights reserved.

Manuscript submitted February 22, 2010; revised manuscript received May 5, 2010. Published June 10, 2010.

The temperature and relative humidity (RH) inside a polymer electrolyte membrane fuel cell (PEMFC) have a significant impact on performance, particularly due to the effect these coupled parameters have on the water balance within the cell.¹⁻⁵ Optimal water balance is achieved when the membrane is well hydrated, ensuring good proton conductivity, and the electrodes are relatively free of liquid water to maintain effective gas transport to the reaction sites.

Water produced at the cathode during cell operation is effective in hydrating the membrane at lower cell temperatures. But at higher operating temperatures, which are preferred for reduced activation polarization, the cathode RH is insufficient and the membrane dries out. Membrane dry-out not only causes an increase in ohmic overpotential but can also accelerate membrane degradation.⁶ To avoid this dry operation, gas streams are typically humidified before entering the cell. Excessive humidification, however, can cause flooding and can severely decrease the cell performance due to mass transport losses. Nonuniformities in the temperature and water distribution are often present⁷⁻⁹ and add to the challenges of thermal and water management.

Further adding to the difficulty of achieving controlled water balance in a PEMFC are dynamic operating conditions, which are common in transportation applications. Recent experimental and modeling studies further elucidate the roles of temperature and humidity on cell performance under these conditions.^{10,11} As predictive models are extended to two and three dimensions, the ability to measure distributed temperature and RH in situ becomes increasingly useful for validation. Techniques developed for these purposes also supplement conventional bulk diagnostic techniques.

Distributed measurements of RH and temperature inside a PEMFC have been performed using electrical and optical techniques with varying degrees of invasiveness and practicality. Microtemperature and humidity sensors were fabricated on a metallic bipolar plate of a PEMFC by Lee et al. for in situ diagnostics.¹² The sensors were calibrated, and polarization curves were reported for an operating fuel cell with and without sensors, indicating a significant drop in performance when sensors were embedded, but no temperature or RH data were presented.

Using tunable laser diode spectroscopy, Basu et al.¹³ claimed the first simultaneous nonintrusive measurements of water vapor partial pressure and temperature inside a PEMFC under steady and tran-

sient operations. Two channels in the serpentine flow path of a bipolar plate were extended to the edges to allow optical access into a test cell. One sensing channel was located near the inlet, and one was located near the outlet. This technique was limited, however, in its temperature resolution, and temperature differences between the two flow channels were not resolved. The partial pressure of water vapor, which is proportional to RH for a given temperature, was measured to increase linearly with cell current and was higher toward the outlet. These measurements agreed with the calculated production of water at the cathode and were not significantly affected by electro-osmotic drag. A similar approach was proposed by Partridge et al.,¹⁴ who reported on the use of spatially resolved capillary inlet mass spectrometry to measure water concentration at multiple locations in the serpentine flow field of an operating PEMFC. The authors suggest that in combination with spatially resolved temperature measurements, the transient RH distributions could also be measured. Data for such measurements, however, were not presented.

The trends in the partial pressure of water vapor across the cell reported in Basu et al. were confirmed more recently by the distributed RH measurements of Hinds et al.¹⁵ In their work, they used miniature single-chip capacitive sensors from Sensirion Inc. (SHT75) to accurately measure temperature and RH at points around the flow field of a single test cell. The sensors, although relatively small, were still too large to be installed directly into the flow channels in the active area and were therefore recessed into auxiliary channels around the active area. The main constraint of this technique was the sensor size (3×7 mm), which limits the ability to make measurements in the active area and limits the transfer of the technique to commercial plate designs.

The focus of the present work is the development of an in situ fiber-optic-based measurement technique that addresses temperature resolution and sensor size limitations of existing methods.^{13,15} Optical fibers have properties that are suitable for the PEMFC environment: In particular, they are nonconductive, chemically inert, and inherently small. They were recently used by Inman et al.¹⁶ for an in situ distributed point measurement of temperature across the surface of the gas diffusion layer. The point sensor they developed, located at the fiber tip, is based on the principle of phosphor thermometry.

In a previous work, we introduced the use of in-fiber Bragg grating (FBG) sensors for distributed temperature measurements in a PEMFC.¹⁷ In contrast to the sensors used by Inman et al., FBGs are installed parallel to the fuel cell plates and can be multiplexed with several sensors on a single fiber. Building on this, in this paper, we

* Electrochemical Society Active Member.

^z E-mail: nadavid@uvic.ca

present an extension of the FBG technique to the simultaneous measurement of RH and temperature. Sensors are fabricated and installed in flow channels of the graphite cathode flow plate of a single PEMFC and used to take minimally invasive measurements during cell operation. With the addition of FBG multiplexing, the technique presented here offers the prospect of real-time multipoint monitoring of complete stacks.

Fiber Bragg Gratings: Background

An FBG typically consists of a short segment of a single-mode optical fiber with a photoinduced periodically modulated index of refraction in the core of the fiber. This effectively creates a grating of planes perpendicular to the fiber axis. When the grating is illuminated with broad-band light, the reflected power spectrum has a structure caused by interference of the light with the planes of the grating. The peak of the spectrum occurs at the Bragg wavelength, $\lambda_B = 2\Lambda n$, where n is the index of refraction of the silica fiber and Λ is the grating pitch. When grating is subjected to mechanical or thermal strain, its pitch changes, causing a shift in Bragg wavelength.

This shift is given by

$$\frac{\Delta\lambda_B}{\lambda_B} = (1 - Pe)\varepsilon + [(1 - Pe)\alpha + \xi]\Delta T \quad [1]$$

where Pe is the photoelastic constant of the fiber, ε is the mechanical strain induced in the fiber, α is the coefficient of thermal expansion of the optical fiber, and ξ is the thermo-optic coefficient. A comprehensive review of FBGs, along with a description of many of their important applications, can be found in Rao.¹⁸

One such application is RH sensing.¹⁹⁻²¹ FBG is coated with a moisture-sensitive polymer that swells as water vapor absorbs into micropores of the material. Swelling of the polymer causes axial strain in the FBG, which is proportional to RH.

In the absence of external mechanical strain, the Bragg wavelength shift can be represented as a linear superposition of response to changes in RH (ΔRH) and temperature (ΔT)

$$\frac{\Delta\lambda_B}{\lambda_B} = S_T\Delta T + S_{RH}\Delta RH \quad [2]$$

where the temperature and RH sensitivity coefficients, S_T and S_{RH} , are given by

$$S_T = (1 - Pe) \frac{E_p(r_f + t)^2}{E_p(r_f + t)^2 + E_f r_f^2} (\alpha_p - \alpha_f) + \xi_f \quad [3]$$

$$S_{RH} = (1 - Pe) \left[1 - \frac{E_f r_f^2}{E_f r_f^2 + E_p(t^2 + 2tr_f)} \right] \beta_p \quad [4]$$

These coefficients were calculated based on a uniform axial strain model, neglecting edge effects.^{19,21} The variables α_p , β_p , E_p , and t represent the coefficients of thermal and hygroscopic expansion, the Young's modulus, and the thickness of the polymer material. The Young's modulus and the radius of the fiber are represented by E_f and r_f , and ξ_f is the thermo-optic coefficient of the fiber.

This type of sensor with the moisture-sensitive polyimide Pyralin (PI-2525 from HD Microsystems) was first presented by Kronenberg et al.¹⁹ The authors showed that an FBG coated with polyimide has a linear and reversible response for temperature and RH ranges of 13–60°C and 10–90%, respectively. The highest temperature in their study was limited to the maximum operating range of the electrical gauge used, and they report additional tests showing that the sensor was not damaged when exposed to temperatures ranging from –20 to 160°C. In a similar study by Yeo et al.,²⁰ Pyralin-coated sensors were characterized with linear response up to an RH level of 97%. The ranges reported by both groups suggest good compatibility of the sensors in a PEMFC.

In both the work of Kronenberg et al. and Yeo et al., several sensors were fabricated from standard single-mode fiber (SMF 28) FBGs, each with a different coating thickness, and were tested in a

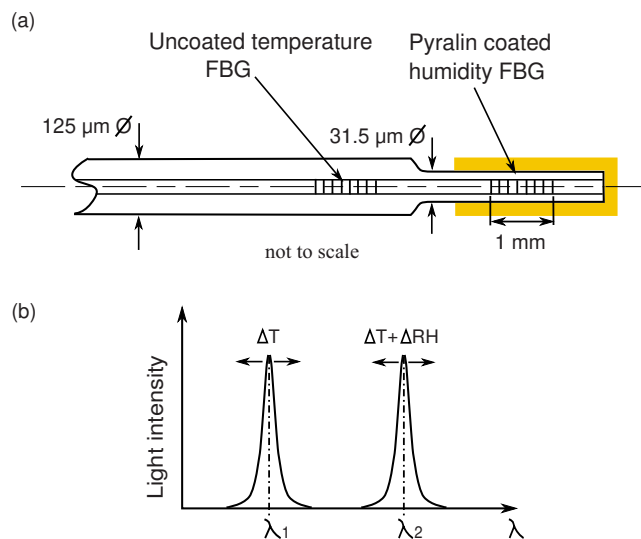


Figure 1. (Color online) (a) Schematic of the RH sensor consisting of two 1 mm FBGs spaced apart by 3 mm. The distal FBG has a reduced diameter coated with the humidity-sensitive polymer, Pyralin, while the other FBG is left unetched and used for temperature compensation. (b) Schematic of the reflected spectrum from the sensor. The uncoated FBG used for temperature compensation has the Bragg wavelength denoted by λ_1 , which only shifts with temperature. The etched and coated FBG has Bragg wavelength λ_2 and shifts with both RH and temperature.

climatic chamber for sensitivity to temperature and RH. Using these results and published values for other parameters in Eq. 3 and 4, the coefficients of thermal and hygroscopic expansion were identified.

The coating thicknesses tested by Kronenberg and co-workers ranged from ~4 to 30 μm with measured RH sensitivities ranging over an order of magnitude, from 0.3 to 3.0 pm %⁻¹. Temperature sensitivity ranged from 10.0 pm °C⁻¹ for a bare fiber to 12.3 pm °C⁻¹ for the thickest coating.

Based on the sensitivities measured by Kronenberg et al. for the Pyralin-coated sensor, the maximum Bragg wavelength shift for a 100% change in RH would be 300 pm. The same order of magnitude Bragg wavelength shift would result from temperature changes of around 30°C. Controlled temperature increases on this scale are common in PEMFCs when bringing the cell up to operating temperatures, after which point smaller variations can occur during normal operation. To decouple the Bragg wavelength shift due to these temperature variations and to make accurate measurement of RH within the PEMFC environment, temperature compensation is required.

The work of Kronenberg suggests using thicker coatings to enhance sensitivity but does not discuss the impact this might have on the sensor time response, which is also an important consideration for use in a PEMFC. Yeo et al. built upon this work, characterizing the time response of the Pyralin-coated FBG RH sensor to step changes in humidity.²⁰ The response times were 18–45 min for 10–45 μm thick Pyralin coatings, much too long for the investigation of transients in a PEMFC, which are typically on the order of seconds.²² To reduce the response time of the sensor, thinner coatings must be used, but at the cost of lower sensitivity.

According to Eq. 4, however, sensitivity can be re-established by reducing the fiber diameter. In the present work, an FBG-based sensor is fabricated with reduced fiber diameter and temperature compensation, both important features for implementation inside a PEMFC.

Sensor Fabrication and Characterization

A schematic of one of the RH sensors fabricated for this work is shown in Fig. 1a. It is made up of two 1 mm FBGs spaced by 3 mm. The distal FBG was etched and coated with Pyralin for hu-

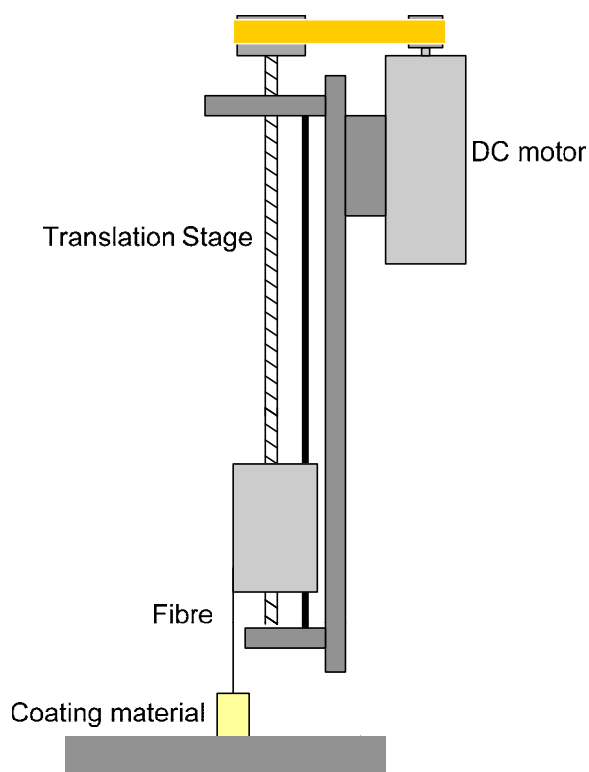


Figure 2. (Color online) Schematic of the dipping procedure used for coating the FBGs with polymer.

midity sensing. The proximal FBG was left unetched and used for temperature compensation, which was necessary due to the dual sensitivity of the coated FBG. The FBGs used for these sensors were written on SMF 28 fiber with Bragg wavelengths of 1540 and 1550 nm and recoated with polyimide for durability (Technica SA Inc., Beijing, China). Depicted schematically in Fig. 1b is a reflected spectrum with two peaks centered on the Bragg wavelengths of each FBG.

A length of fiber with the two FBGs was cut so that one FBG is 2 mm from the distal end. The stock polyimide recoat was removed by immersion in 98% sulfuric acid for approximately 10 min. The fiber was then rinsed in deionized water. To prepare the fiber for HF etching, it was placed in a Teflon tube such that the distal FBG was protruding. Hot wax was used to seal the tube at the midpoint between the two FBGs. The exposed FBG was submerged in 48% HF for 30 min and then immediately neutralized in a saturated CaOH solution to stop the etching. This results in a fiber diameter of $31.5 \pm 0.5 \mu\text{m}$, measured using an optical microscope with a graticule.

For applying the Pyralin coating on the etched FBG, the procedure outlined in Yeo et al. was followed.²⁰ The etched FBG was first wiped with isopropyl alcohol and then dipped in Pyralin and withdrawn at a predetermined constant speed. A speed of 20 mm/min was used to produce uniform coatings without bead formation. A schematic of the setup for coating the FBGs is shown in Fig. 2. Each coat was precured in an oven for 5 min at 150°C. For the sensors in this work, three coats of polymer were applied to obtain a thickness of $2.5 \pm 0.5 \mu\text{m}$. The final baking of the fiber was at 200°C for 1 h.

Calibration of the sensors to RH was carried out using a series of small chambers containing saturated salt solutions to produce humidity fixed points that are in accordance with ASTM 104-02.²³ In this way, the individual sensors, before installation in the fuel cell, are characterized in terms of sensitivity and temporal response to humidity. The temperature calibration of the sensors was conve-

Table I. RH fixed points for the saturated salt solutions used for sensor calibration.²⁴

Salt	RH at 25°C
K ₂ CO ₃	43.16 ± 0.39
NaBr	57.57 ± 0.4
KI	68.86 ± 0.24
KCl	84.34 ± 0.26

niently performed in situ where dry gas can be easily flowed through the channels to create a low constant humidity environment.

Nalgene bottles with a volume of 125 mm were modified so as to accept a single sensor via a Lure lock connection in the lid. The bottles were partially filled with ~25 mm of the saturated salt solutions and then placed in a constant temperature water bath set at 25°C. The four salts used for calibration are listed in Table I, along with their associated RH at 25°C.²⁴ The RH inside the chambers was measured using a Sensirion Inc. SHT75 RH sensor with specified accuracy of ±1.8% RH. The Bragg wavelength shift of the FBG was detected using an optical interrogation unit (SM130 from Micron Optics, Inc., Atlanta, GA), with a specified wavelength resolution of 0.1 pm at a 10 Hz sampling rate.

The time response of the sensor was tested by moving it between two of the bottles containing different salt solutions, the act of which takes less than 2 s.

The RH calibration results for a 31.5 μm diameter fiber FBG with a $2.5 \pm 0.5 \mu\text{m}$ Pyralin coating are shown in Fig. 3. The sensitivity to RH was $0.99 \text{ pm } \% \text{ RH}^{-1}$ from the slope of the linear fit to the data. Although a saturated salt solution for a higher humidity level was not used, linear response for a Pyralin-coated FBG was shown up to 97% RH by Yeo et al. Furthermore, when the sensor was immersed in water, it measured $100 \pm 2.0\%$ RH and recovered quickly upon drying. For this fiber diameter and coating thickness, including their measured uncertainties, the calculated sensitivity based on Eq. 4 is $1.25 \pm 0.25 \text{ pm } \% \text{ RH}^{-1}$, indicating a reasonable agreement between the model of Kronenberg et al. and this etched sensor design. The sensitivity measured here is more than 3 times higher than the value reported by Kronenberg et al. for a $3.6 \pm 1 \mu\text{m}$ thick coating on an unetched fiber.

Figure 4 shows the sensor response to a step change in humidity from 43 and 84% RH. From this plot, the two conventionally defined response times are determined and given in the inset table. The 90% response time of 10 s is a vast improvement over the previous generation of unetched sensors reported in Ref. 20 and is suitable to measure transient phenomena inside a PEMFC. In fact, the 63%

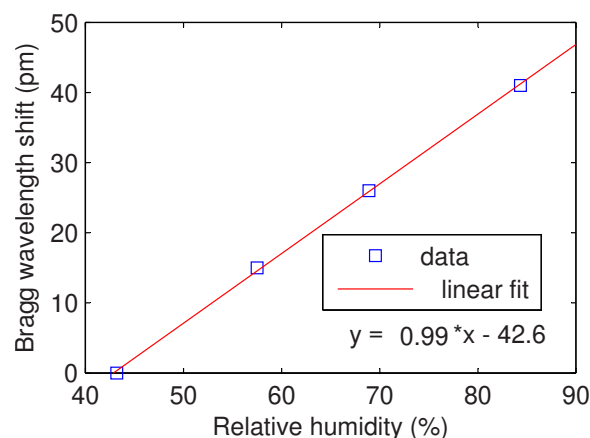


Figure 3. (Color online) RH calibration data for a 34 μm RH sensor acquired using humidity fixed point chambers containing saturated salt solutions.

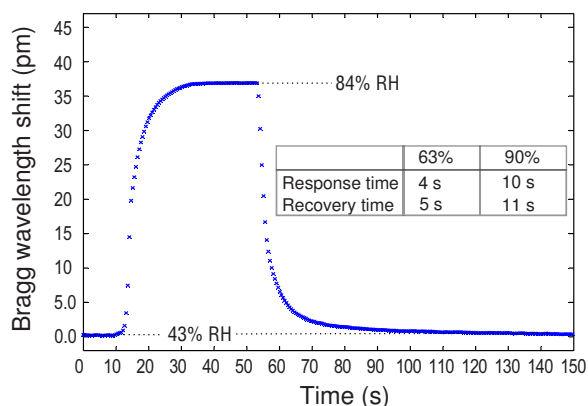


Figure 4. (Color online) Response of the etched sensor with coating thickness of $2.5 \pm 0.5 \mu\text{m}$ to a step change in RH. Conventionally defined response times for the sensor are shown in the table.

response time is half that specified for the commercial sensors used in Ref. 25. Also notable in the response data is that upon returning to the low humidity state, the Bragg wavelength settles back to the original value, indicating reversibility of the polymer expansion mechanism.

Temperature calibration was done with the sensors installed in the graphite fuel cell flow plate. Two miniature T-type thermocouples were installed into a blank graphite plate such that when it is used to cover the flow plate with the FBGs, the thermocouples and the FBGs are colocated. The single cell was assembled, with the blank plate used in place of the membrane electrode assembly (MEA) and the anode flow plate. Dry air was fed into the cathode flow field, and the temperature was increased using the water heating system and then allowed to cool to room temperature by natural convection.

Shown in Fig. 5 are temperature calibration data for each FBG acquired during slow thermal cycling of the sensors in situ under dry conditions. As indicated by the slopes of the linear fits to the data, the polymer coating on the RH-sensitive FBG has the effect of increasing its sensitivity to temperature by $\sim 10\%$. This result is consistent with Eq. 3. Although the calibration was performed in the 25–80°C range, to cover the operating range of interest of the fuel cell, the sensor temperature range can be easily extended.¹⁹

With good linearity and reversibility in the RH and temperature calibration data, estimations of the accuracies of the etched FBG sensors fabricated in this work are $\pm 2.0\%$ RH and $\pm 0.2^\circ\text{C}$. These values are based on the specifications of Sensirion SHT75 and the Omega thermocouple used as references for calibration. The absolute temperature uncertainty reported here is an order of magnitude improvement over that of the technique used by Basu et al. for their in situ measurements¹³ and is adequate to investigate temperature differences between adjacent channels inside a single PEMFC.^{13,17} Resolving differences in temperature and RH in situ is further improved by the high wavelength resolution of the Micron Optics SM130 used to interrogate the FBGs in the sensor. Based on this, the minimum detectable change in RH is 0.1% RH, assuming temperature compensation.

In Situ Experiments

Sensor installation.— A graphite flow plate for a single test cell of an active area of 30.25 cm^2 was machined with a serpentine flow field and instrumented with two of the previously discussed FBG RH sensors. The schematic in Fig. 6a shows the location of one of the installed sensors in the flow plate and where it sits relative to the main PEMFC components. The design challenges in embedding the FBG sensor in an operating fuel cell were discussed in Ref. 17. To avoid interference with the flow in the gas channel, the sensor was installed in a groove at the bottom of the flow channel, as shown in

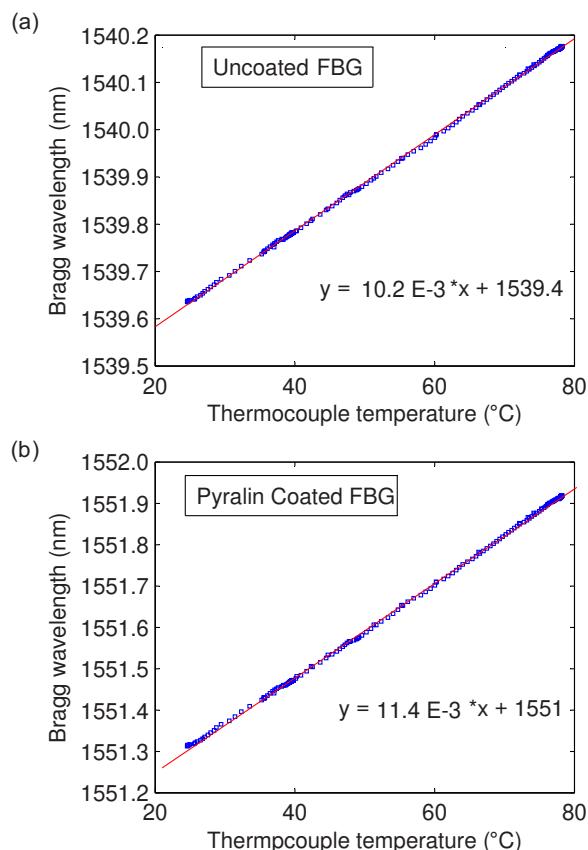


Figure 5. (Color online) Calibration data for the RH sensor with respect to temperature acquired under dry conditions. (a) $125 \mu\text{m}$ uncoated FBG used for temperature compensation. (b) $34 \mu\text{m}$ Pyralin-coated FBG.

Fig. 6b. Underneath the sensor is a recess in the groove to ensure that the entire surface of the sensor is in contact with the air in the channel. Clearly, from the figure, with this installation and with the small diameter of the sensor, there is minimal impact on the active area of the PEMFC.

Proper sealing of the installation is also important to minimize the impact on performance. Cyanoacrylate adhesive was used to fix the fiber in place and to seal the angled hole where it enters the flow channel. This provides strain relief to ensure that only the changes in RH and temperature within the sensing region are detected rather than mechanical strain transmitted from the exterior. Another important feature of the design shown in Fig. 6b is the curve in the fiber as it enters the sensing region from outside the cell. Excessive bending results in loss of optical power transmitted to and from the sensor, and bends therefore should be limited to about 1 cm in radius.

Figure 7 shows the locations of the two sensors along the flow field in the graphite flow plate. The plate is used on the cathode side of the test cell, and air flows over sensors 1 and 2 from the inlet to the outlet, respectively.

Test cell.— The instrumented graphite plate described above was sized to fit into a pre-existing fuel cell test assembly. The assembly consists of gold-plated current collector plates, and stainless steel manifolds for gas distribution and water circulation for the cell heating system. This assembly can be seen in Fig. 8, where the fiber optics is also shown entering the cathode plate.

MEAs for the test cell were fabricated at the National Research Council Institute for Fuel Cell Innovation, Vancouver, Canada. An active area of 30.25 cm^2 , with platinum loading of 0.4 mg/cm^2 , was achieved by masking and spray deposition of a carbon catalyst ink onto Nafion 115 membrane. The gas diffusion layer used for the

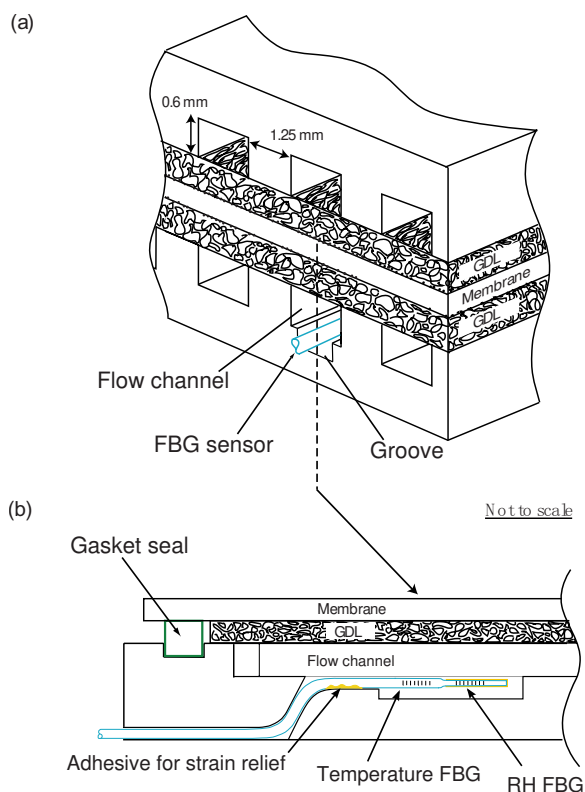


Figure 6. (Color online) Schematic of the in situ FBG sensor located in the bottom of the flow channel of the graphite flow plate (a). The side view schematic in (b) shows how the sensors were installed into the flow plate.

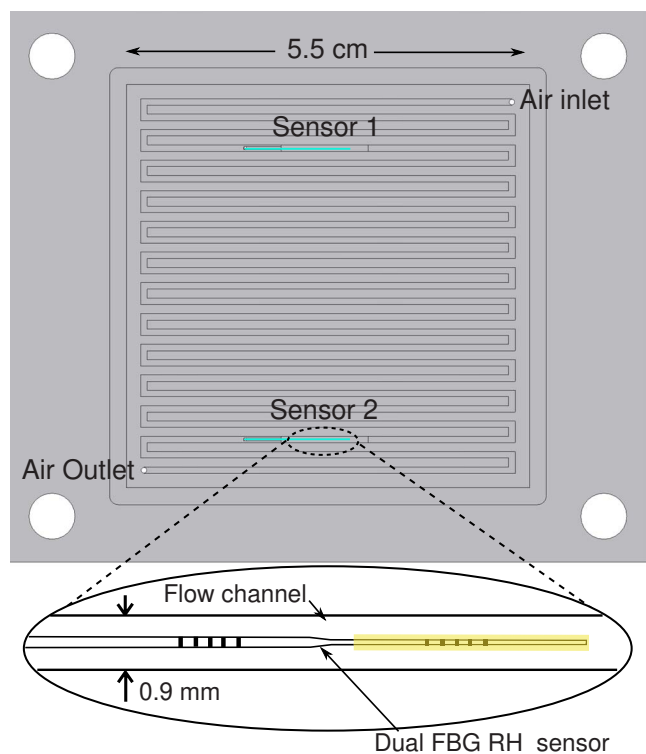


Figure 7. (Color online) Schematic of the cathode flow plate showing the locations of the two etched FBG RH sensors. Inset drawing is of a single sensor embedded in the flow channel.

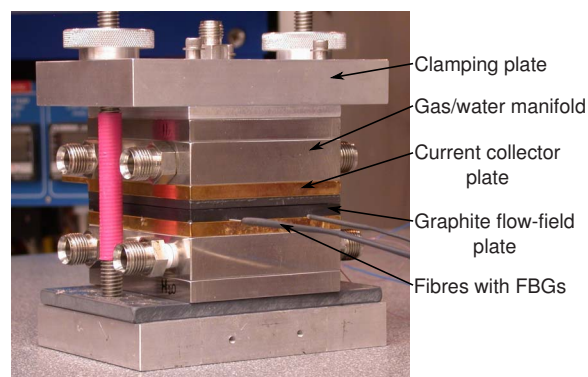


Figure 8. (Color online) Photograph of the single test cell assembly. The cell temperature is set by circulating deionized water from a temperature controlled bath in the test station through the stainless steel plates on either side of the cell.

MEAs was Toray paper with 10% polytetrafluoroethylene content, and that for the MEAs used in this study was not hot-pressed onto the carbon catalyst layer.

The test cell was operated using a Ballard 3 kW fuel cell test station, which enabled control of the fuel and oxidant flow rates, and a cell temperature with a water heating system. The current density of the fuel cell was varied using an electronic load bank (Dynamload Inc., MCL488, Hackettstown, NJ) that was connected via copper leads to the gold-plated collector plates on either side of the single cell. The cell voltage was measured using analog inputs on a 16 bit data acquisition device (National Instruments Inc.).

In situ testing conditions.— For in situ testing of the sensors, the cell was run in the coflow mode with the temperature set to 40°C. Water tanks for the gas humidifier were also set to 40°C, but because the tubing from these tanks to the test cell was not heated, the inlet gas streams were underhumidified. A standard PEMFC test is to vary the cell current with the load and to acquire a polarization curve by measuring the corresponding cell voltages. By performing this test with the sensors installed, steady-state and transient behaviors are observed in the cell voltage as well as in the RH and temperature within the cell. Data from the sensors were acquired at a sampling rate of 1 kHz and presented with 1000 averages to improve the resolution. Before carrying out the current sweeps for polarization tests, the MEA was conditioned by running the cell at 0.3 A cm⁻² for ~30 min.

Results and Discussion

To obtain a polarization curve quasi-statically, the cell current was incremented from 0 to 15 A and back down to 0 in steps of 3 A, allowing the cell voltage to reach steady state between each step. The flow rates for the air and hydrogen streams were set to 1.25 and 0.75 slpm. This overstoichiometry was used to prevent water accumulation in the flow channels. Because the etched fiber sensor is free at one end in this installation, the fine fiber can be easily deflected due to the surface tension of water accumulated around it. The resulting strain on the FBGs perturbs the sensor measurements significantly. Such perturbations were observed at low oxidant flow rates and higher currents.

Results from incrementally increasing the cell current from 0 to 15 A are shown in Fig. 9 with the cell voltage data and the sensor measurements. In Fig. 9b, the RH near the outlet climbs higher than the inlet RH after the first step in cell current. The following two steps in current, to 6 and 9 A, are also marked with increases in RH near the outlet. Subsequent steps in current result in smaller increments in RH near the outlet until a maximum of around 90% RH is reached.

In contrast to the large changes in RH near the outlet, the inlet RH increases in smaller steps. These steps continue throughout the

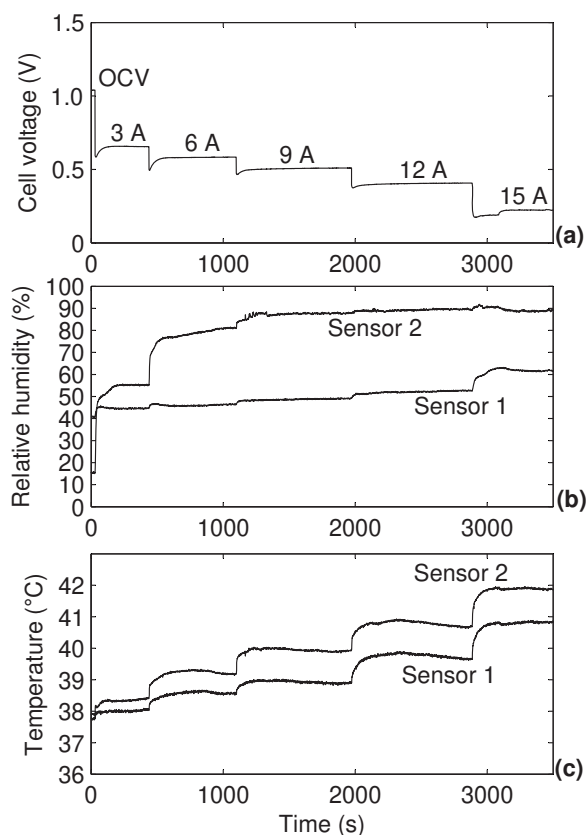


Figure 9. (a) Voltage, (b) RH, and (c) temperature data taken while incrementing cell current for obtaining a polarization curve. The flow rates for the air and hydrogen were 1.25 and 0.75 slpm, respectively.

range of currents with no plateau, as is the case for the outlet RH. The higher RH measured near the outlet on the cathode side for all cell currents above zero is to be expected; water produced in the catalyst layer during cell operation acts to increasingly humidify the air as it flows from the inlet to the outlet. Sensor 1 is only a few channels downstream from the inlet and, therefore, measures air that has a limited interaction with product water and has thus generally lower RH.

Shown in Fig. 10 is the transient response of sensor 2 following a step change in current from 0 to 3 A, with the cell voltage response plotted for comparison. There is an initial rise in RH of more than

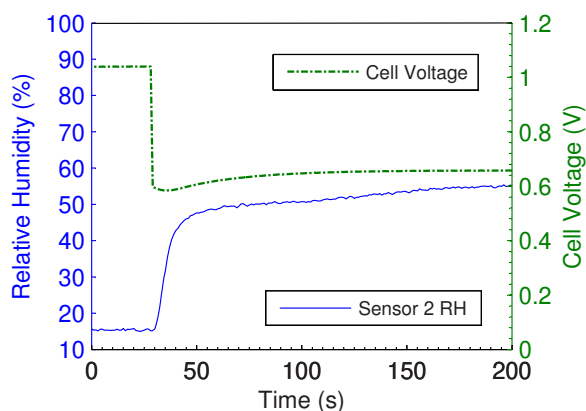


Figure 10. (Color online) Transient response of sensor 2 following a step change in current density from 0 to 3 A at time $t = 28$ s. The cell voltage response is also shown for comparison.

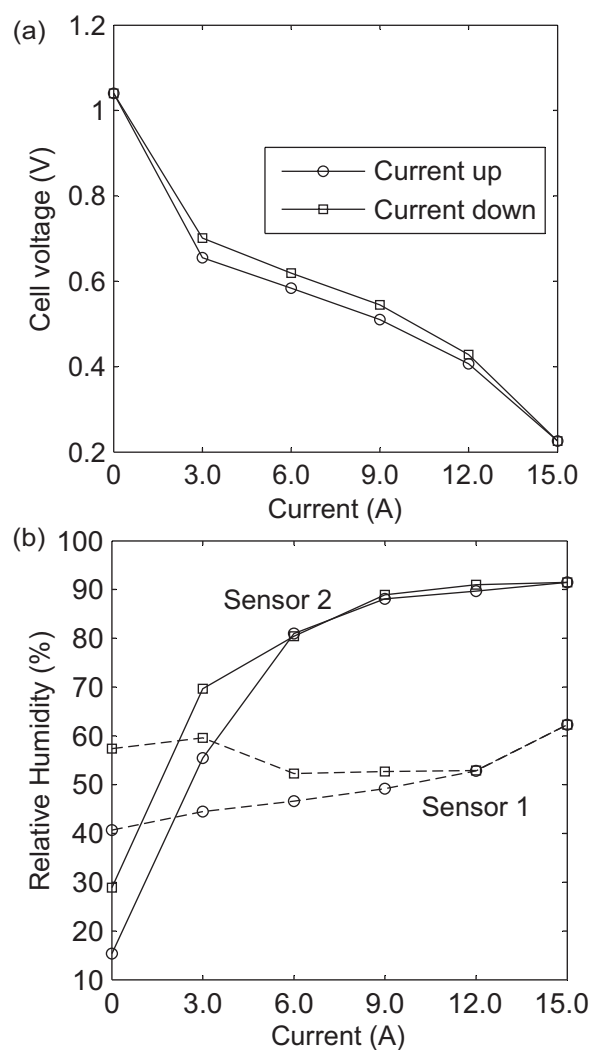


Figure 11. (a) Steady-state polarization data for increasing and decreasing currents with cell temperature set to 40°C. (b) Corresponding steady-state RH measurements of sensors 1 and 2.

30% in ~ 30 s after the step change. This is followed by a smaller and slower increase in RH, after which it reaches steady state at a time comparable to the cell voltage ($t = \sim 180$ s). The response of the cell voltage and the RH agrees with measurements of Hinds et al. and is consistent with the time scale of water sorption into the Nafion membrane, which is of the order of hundreds of seconds.²⁶ This result demonstrates that RH transients inside a PEMFC exist on a time scale approaching the sensor response time and that the sensor could provide information on the dynamics of water transport in the MEA.

Temperature differences, reaching up to $\sim 1.5^\circ\text{C}$, were also measured in the flow field between the inlet and the outlet, as shown in Fig. 9c. These are expected as a result of higher membrane hydration toward the outlet, leading to higher current densities and more ohmic losses. Gradients in temperature such as this have also been reported in other studies.^{17,27,28}

The steady-state polarization results for the test described are shown in Fig. 11. The cell voltage measured for decremented current is higher than that for the incremented current, indicating hysteresis in performance. The corresponding steady-state measurements of RH are shown in Fig. 11b, which also show hysteresis and likely contribute to the hysteresis in the polarization curve.

Conclusions

An etched fiber, polymer-coated FBG sensor for a fast response, high sensitivity measurement of RH and temperature has been demonstrated. Two of the sensors were embedded directly into the cathode flow channels of a single test cell and were used to make real-time measurements of RH and temperature during cell operation.

Results show that for an increased current density, much larger increases in RH occur near the outlet than near the inlet, a trend that has been reported in other studies. From the results, it was also determined that RH transients inside a PEMFC exist on a time scale approaching the sensor response time, proving that the sensor could provide information on the dynamics of water transport in the MEA.

The small size of the sensor implemented here and its accurate, high resolution measurement capabilities combine to address key limitations of other techniques used for in situ PEMFC measurements. In the interest of improved cell design, particularly with regard to humidification and thermal and water management schemes, this relatively inexpensive technique could prove useful as a noninvasive in situ diagnostic tool.

Further improvements of the technique involve the multiplexing of several temperature-compensated FBG RH sensors on a single fiber. This increases the number of measurement points from 4 to 10, resulting in truly distributed RH and temperature data within an operating fuel cell. This naturally lends itself to a sensor installation that is fixed on both ends and, therefore, to measurements that are unperturbed by liquid water. Furthermore, with the minimal invasiveness of the optical fibers into the fuel cell flow plate, the technique could be extended for use in bipolar plates for multipoint monitoring of complete stacks.

Acknowledgments

This work was funded by the Natural Sciences and Engineering Research Council (NSERC) of Canada and the Canada Research Chairs program. The authors also acknowledge the valuable input of Dr. Matt Moffit on coating techniques.

University of Victoria assisted in meeting the publication costs of this article.

References

1. J. Lariminie and A. Dicks, *Fuel Cell Systems Explained*, John Wiley & Sons, New York (2000).
2. M. M. Mench, Q. L. Dong, and C. Y. Wang, *J. Power Sources*, **124**, 90 (2003).
3. Q. G. Yan, H. Toghiani, and J. X. Wu, *J. Power Sources*, **158**, 316 (2006).
4. A. Z. Weber and J. Newman, *J. Electrochem. Soc.*, **153**, A2205 (2006).
5. S. Kim and M. M. Mench, *J. Electrochem. Soc.*, **156**, B353 (2009).
6. C. Chen and T. F. Fuller, *Polym. Degrad. Stab.*, **94**, 1436 (2009).
7. N. Djilali and D. Lu, *Int. J. Therm. Sci.*, **41**, 29 (2002).
8. T. Berning and N. Djilali, *J. Electrochem. Soc.*, **150**, A1589 (2003).
9. S. Kjelstrup and A. Rosjorde, *J. Phys. Chem. B*, **109**, 9020 (2005).
10. M. Meiler, D. Andre, O. Schmid, and E. P. Hofer, *J. Power Sources*, **190**, 56 (2009).
11. A. A. Shah, G. S. Kim, P. C. Sui, and D. Harvey, *J. Power Sources*, **163**, 793 (2007).
12. C.-Y. Lee, G.-W. Wu, and C.-L. Hsieh, *J. Power Sources*, **172**, 363 (2007).
13. S. Basu, M. W. Renfro, and B. M. Cetegen, *J. Power Sources*, **162**, 286 (2006).
14. W. P. Partridge, T. J. Toops, J. B. Green, and T. R. Armstrong, *J. Power Sources*, **160**, 454 (2006).
15. G. Hinds, M. Stevens, J. Wilkinson, M. de Posta, and S. Bell, *J. Power Sources*, **186**, 52 (2009).
16. K. Inman, X. Wang, and B. Sangeorzan, *J. Power Sources*, **195**, 4753 (2010).
17. N. A. David, P. M. Wild, J. Hu, and N. Djilali, *J. Power Sources*, **192**, 376 (2009).
18. Y.-J. Rao, *Meas. Sci. Technol.*, **8**, 355 (1997).
19. P. Kronenberg, P. K. Rastogi, P. Giaccari, and H. G. Limberger, *Opt. Lett.*, **27**, 1385 (2002).
20. T. L. Yeo, T. Sun, K. T. V. Grattan, D. Parry, R. Lade, and B. D. Powell, *Sens. Actuators B*, **110**, 148 (2005).
21. X. F. Huang, D. R. Sheng, K. F. Cen, and H. Zhou, *Sens. Actuators B*, **127**, 518 (2007).
22. S. Shimpalee, W.-k. Lee, J. Van Zee, and H. Naseri-Neshat, *J. Power Sources*, **156**, 355 (2006).
23. American Society for Testing and Materials, E104-02 (2007).
24. L. Greenspan, *J. Res. Natl. Bur. Stand., Sect. A*, **81A**, 1 (1977).
25. SHT7x Datasheet, Sensirion Inc., Zurich, Switzerland, <http://www.sensirion.com>, last accessed 2009.
26. P. Majsztrik, M. Satterfield, A. Bocarsly, and J. Benziger, *J. Membr. Sci.*, **301**, 93 (2007).
27. M. Wang, H. Guo, and C. Ma, *J. Power Sources*, **157**, 181 (2006).
28. P. T. Nguyen, T. Berning, and N. Djilali, *J. Power Sources*, **130**, 149 (2004).